



# Emitter localisation from reception timestamps in asynchronous networks



Nicolò Facchi<sup>a</sup>, Francesco Gringoli<sup>a</sup>, Fabio Ricciato<sup>b,c,\*</sup>, Andrea Toma<sup>c</sup>

<sup>a</sup> Department of Information Engineering, CNIT—University of Brescia, Brescia, Italy

<sup>b</sup> Faculty of Computer and Information Science, University of Ljubljana, Ljubljana, Slovenia

<sup>c</sup> Austrian Institute of Technology, Vienna, Austria

## ARTICLE INFO

### Article history:

Received 4 November 2014

Revised 11 April 2015

Accepted 9 June 2015

Available online 16 June 2015

### Keywords:

Time-based localisation

Asynchronous networks

Opportunistic localisation

WiFi testbed

## ABSTRACT

We address the problem of localising a mobile terminal (“blind” node) in unknown position from a set of “anchor” nodes in known positions. The proposed method does not require any form of node synchronisation nor measurement (or control) of the transmission times, which is difficult or anyway costly to achieve in practice. It relies exclusively on reception timestamps collected by the anchor nodes, according to their local clocks, that overhear packets transmitted by the blind node and by (at least one) other transmitting node(s) in known position, e.g., other anchors. The clock differences between the nodes are not eliminated *ante* through clock synchronisation, as in traditional ToA and TDoA methods. Instead, they are counteracted *ex post*, during the data processing stage, leveraging the data redundancy that is intrinsic to the multiple reception of the same packet by different (anchor) nodes. We validate the proposed method in different experimental settings, indoor and outdoor, using exclusively low-cost Commercial-Off-The-Shelf WiFi devices, achieving sub-metre accuracy in full line-of-sight conditions and metre-level accuracy in mild non-line-of-sight environment. The proposed method does not require that the blind node participate actively to the localisation procedure and can use “opportunistically” any legacy signal or packet available over-the-air for communication purposes. Considering the very minimal requirement on the system—basically, only that anchors in known positions are able to collect and share reception timestamps—the proposed approach can enable practical adoption of opportunistic and/or cooperative localisation on top of existing radio communication systems.

© 2015 Published by Elsevier B.V.

## 1. Introduction

Despite the widespread success of Global Navigation Satellite Systems (GNSS), alternative radio-based positioning systems remain of interest for those applications where GNSS signals are not available (e.g., indoor, tunnels, urban canyon) and/or the integration of GNSS receivers is not feasible due to size, energy or cost constraints. In order to pre-

serve cost-effectiveness and ease of adoption, it is desirable to develop localisation methods that reuse *opportunistically* the legacy radio signals, protocols and receivers which are anyway available for communication purposes. We consider the problem of localising a transmitting node in unknown position, called “blind node” hereafter, based on the reception measurements collected by a set of nodes in known positions, called “anchors”.

One possible approach is to rely on *power* measurements, leveraging the Received Signal Strength Indicator (RSSI) available today in almost all Commercial Off-The-Shelf (COTS) transceivers to deploy RSSI-based localisation functions on top of existing wireless communication

\* Corresponding author at: Faculty of Computer and Information Science, University of Ljubljana, Večna pot 113, SI-1001 Ljubljana, Slovenia. Tel.: +386 14798285.

E-mail address: [fabio.ricciato@fri.uni-lj.si](mailto:fabio.ricciato@fri.uni-lj.si) (F. Ricciato).

systems. Both commercial and open-source tools are available for several technologies, including WiFi, Bluetooth, and IEEE 802.15.4 (e.g. [1–3]). Generally speaking, RSSI-based methods exhibit low accuracy, since in real environments the received power is heavily affected by other factors than the distance from the transmitter, most prominently multipath propagation and antenna patterns. Several previous work seek to improve accuracy of RSSI-based methods using machine learning techniques that create and use detailed power loss maps for specific environments [4–7], in the direction of so called “RSSI fingerprinting” techniques.

Another class of approaches is based on *time* measurements. As signals travel at constant speed, the relation between reception time and distance is tighter than for received power, therefore time-based localisation is intrinsically superior to RSSI-based methods in terms of potential accuracy [8]. However, the traditional approaches to time-based localisation require the system to support some form of *node synchronisation* and/or accurate *measurement or control of transmission times*. Both these functionalities are difficult or costly to achieve in practice [9]. Node synchronisation requires the distribution of synchronisation signals, either via additional wired infrastructure or wireless protocols, and the implementation of dedicated functions into the devices which consume additional energy, bandwidth, and computation resources [9]. Controlling or measuring the actual transmission time is also difficult with standard hardware, due to unpredictable delay components between the construction of the packet and the transfer to the network interface on one hand, and the intrinsic variability of channel access delays due, e.g., to MAC dynamics [9]. For these reasons we are interested in time-based localisation methods that (i) do not require any synchronisation across nodes and (ii) do not rely on knowledge nor control of *transmission times*.

In standard time-of-arrival (ToA) methods all nodes must use a common synchronous clock reference and must take active part to the localisation procedure [8,10,11]. The transmitting node attaches a transmission timestamp to the packet in order to allow the receiver to compute the travel time (also called “time of flight”) and from there derive the distance from the transmitter (one-way ranging). In two-way ranging methods instead, node A sends a probe packet to node B and the latter answers back with a reply packet that includes the information about the elapsed time between the reception of the probe and the transmission of the reply packet (also called “turn-around time”). By subtracting this value from the elapsed time between the transmission of the probe packet and reception of the reply packet, node A is able to compute the distance (range) to B. Two-way ranging does not need clock synchronisation between the nodes, however it still requires accurate knowledge of (the difference between) pairs of *transmission and reception times*. Moreover, it requires that the node to be localised (“blind node”) take active part into the ranging phase [12]. With time-difference of arrival (TDoA) methods an emitter node can be localised by a set of anchors in known positions that measure exclusively the reception times of the signals transmitted by the blind node [13]. This method relaxes the requirement on the transmission times, but still needs tight synchronisation between the anchor nodes for accurate localisation [14].

Due to the requirements on node synchronisation and/or measurement or control of transmission time, it is impractical to deploy these methods on COTS devices [15–18]. To overcome these limitations, we consider here a localisation method that *relies exclusively on reception timestamps and does not require any form of node synchronisation*. The proposed method can passively localise a (possibly unaware) blind node while it is executing standard communication operations, i.e., exchanging packets with a neighbouring node, without requiring its active participation to the localisation procedure. In other words, our method meets all the following system-level requirements:

- The blind node transmits beacons and/or packets (e.g. towards one or more other nodes, mobile or fixed) but it does not take any active part to the localisation process. The localisation procedure involves exclusively a set of “anchor” nodes in known positions.
- No synchronisation mechanism is in place between the anchor nodes nor between blind and anchors, i.e., we assume *asynchronous nodes*.
- Anchor nodes can measure only local *reception times* (i.e., timestamps) while the *transmission times* are unknown and cannot be controlled, i.e., we assume *asynchronous signals*.

It can be easily seen that the above requirements do not allow to adopt ToA, two-way ranging, TDoA nor other hybrid variants proposed recently in the literature (e.g. [18–24]) that anyway demand some combination of node synchronisation, knowledge and/or control of transmission times and blind node involvement.

By fulfilling the above requirements, the method described here can be adopted in a wide range of practical applications to localise passively a mobile transmitter based exclusively on the *local reception timestamps* collected by other nodes placed in the surrounding environment. Waiving the requirements of node and signal synchronisation enables the implementation of localisation capabilities in legacy communication systems, which are typically completely asynchronous. Possible applications include indoor localisation of smartphones, customer tracking for retail marketing intelligence [25], localisation in wireless sensor networks (WSN), and extension (augmentation) of GNSS positioning in Cooperative Intelligent Transportation Systems (C-ITS) [26].

While in traditional localisation systems clock differences are eliminated *ex-ante* by the synchronisation mechanism, we consider a model where clock differences are accounted for *ex-post*, i.e., they are either cancelled or estimated during the data processing stage, jointly with the estimation of the (unknown) blind position. This approach is conceptually similar to the well-known “double-difference” method used in GNSS to eliminate residual errors on the carrier *phase* for high-precision applications (see e.g. [27]). Only a few recent pioneering works have started to consider this class of techniques for *time* (instead of phase) measurements in the context of terrestrial (not GNSS) localisation systems [28–34]. The method elaborated here belongs to the class of so-called *differential* time-difference of arrival (DTDoA). A detailed review of previous DTDoA literature is given later in the Related Work section. The main goal of our contribution is to demonstrate that DTDoA localisation can deliver sub-metre

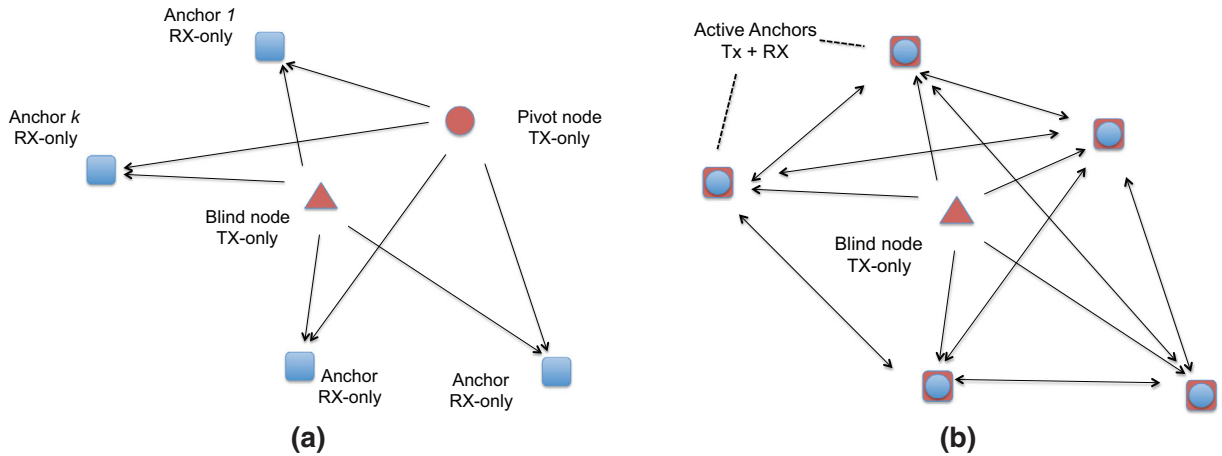


Fig. 1. Reference scenarios. (a) Basic scenario with multiple receive-only anchors and a single pivot node. (b) Extended scenario with multiple active anchors.

accuracy (in line-of-sight conditions) using exclusively COTS receivers, without any additional clock synchronisation mechanism. To this end, we present for the first time experimental measurements obtained with a testbed setting consisting exclusively of COTS WiFi devices, in both indoor and outdoor environments.<sup>1</sup>

The rest of this paper is organised as follows. In Section 2 we formalise the system model and describe step-by-step the proposed methodology in the basic scenario of receive-only anchors. In Section 3 we provide experimental results with COTS WiFi devices in two different testbed scenarios, indoor and outdoor, achieving metre-level accuracy. In Section 4 we extend the method to work in scenarios with multiple active anchors that are able also to transmit (in addition to receive) packets: our experimental results show that the positioning accuracy can be improved down to sub-metre level if all nodes are in line-of-sight (LOS). In Section 5 we extend our method to take advantage of frequency diversity via multi-channel measurements, in this way we can maintain metre-level accuracy also in mild non-line-of-sight (NLOS) conditions. In Section 6 we discuss future research directions for progressing and extending the work. In Section 7 we position our method with respect to existing literature. Finally, we conclude in Section 8.

## 2. Methodology

### 2.1. System model

For the sake of simplicity we consider a 2D localisation problem, being the extension to 3D localisation quite straightforward.

The basic reference scenario represented in Fig. 1(a) involves three types of radio nodes: the *blind node*, one *pivot node* and a set of (minimum three) *anchors*. The positions of the pivot node and of all anchor nodes are known, and the goal is to estimate the (unknown) position of the blind node.

We consider a basic scenario where the blind and pivot nodes emit packets that can be overheard and timestamped by the anchor nodes. In other words, for the purpose of collecting timing measurements, the anchors act as passive receivers (Rx-only) while the blind and pivot act as pure emitters (Tx-only). No synchronisation method is adopted, i.e., the system is completely asynchronous. In a nutshell, the role of the pivot node is to provide reference signals (packets), transmitted from a known location, that compensate the lack of synchronisation between the anchors. In practical setting, the blind and pivot nodes could map, respectively, to a mobile terminal (e.g. smartphone) and to a fixed Access Point (e.g. WiFi or Bluetooth). These two nodes normally exchange data and acknowledgment packets between themselves, however they are not required to take active part in the localisation procedure, i.e., they do not need to perform any additional function besides the standard communication protocol operations. On the anchor side, the only requirement is that they timestamp every received packet and communicate the collected timestamps and the associated packet identifiers to a central computation server in charge of running the localisation algorithm, taking in input the (known) positions of the anchor and of the pivot.

For the sake of simplicity we consider here a centralised scheme and a fully trusted environment, where measurement data and computation are concentrated in a single central server, and all the input data are correct (up to unintentional measurement errors) and shared openly. However, considering that the proposed algorithm consists of a series of simple linear operations, it should be possible to develop more sophisticated variants amenable to distributed computation, possibly taking into account additional requirements for preservation of sensitive data (e.g. anchor node location) and/or robustness against malicious users. These aspects fall outside the focus of the present work and are left as prominent directions for future research.

### 2.2. Notation and basic equations

With reference to the basic scenario depicted in Fig. 1(a) we introduce the following notation. We shall use the

<sup>1</sup> The experimental dataset used in this work along with the software developed to setup the testbed can be obtained from <http://www.ing.unibs.it/~openfwf/localisation>.

symbol “\*” and “o” to label the variables (e.g. transmission and reception times) associated with packets transmitted by the blind and pivot node, respectively. Anchor nodes are indexed in  $k$ , with  $k = 1, \dots, K$ , and  $K \geq 3$  denotes the total number of available anchors. We define the following variables:

- $t_i^*$  [resp.  $t_i^o$ ] denotes the *transmission time* (according to an ideal absolute clock) of the  $i$ th packet transmitted by the blind node [resp. pivot].
- $r_{i,k}^*$  [resp.  $r_{i,k}^o$ ] denotes the *reception time* (according to an ideal absolute clock) at anchor node  $k$  of the  $i$ th packet transmitted by the blind node [resp. pivot].
- $s_{i,k}^*$  [resp.  $s_{i,k}^o$ ] denotes the *reception timestamp* recorded at anchor node  $k$  according to its local clock for the  $i$ th packet transmitted by the blind node [resp. pivot].
- $\mathbf{p}$ ,  $\mathbf{p}^o$  and  $\mathbf{p}_k$  denote the position vectors, respectively of the blind, pivot and generic  $k$ th anchor.
- $d_k \stackrel{\text{def}}{=} \|\mathbf{p} - \mathbf{p}_k\|$  and  $d_k^o \stackrel{\text{def}}{=} \|\mathbf{p}^o - \mathbf{p}_k\|$  denote the Euclidean distances between anchor  $k$  and, respectively, the blind node and pivot node.

The proposed method is based on the estimation of range differences among subsets of four nodes—hereafter referred to as “quadruplets”—consisting of a pair of transmitters, namely the blind node and the pivot, and a pair of receiving anchors. A generic quadruplet is depicted in Fig. 2. One of the  $K$  anchor nodes shall serve as main reference: without loss of generality we pick the first anchor, with index  $k = 1$ , as the reference anchor. Since all quadruplets have three nodes in common—blind, pivot and reference anchor—and differ only for the remaining anchor, we obtain  $K - 1$  quadruplets. For each anchor (equivalently: quadruplet)  $k \in \{2, \dots, K\}$  we define the following *differential ranges*:

$$\Delta_k \stackrel{\text{def}}{=} d_k - d_1 = \|\mathbf{p} - \mathbf{p}_k\| - \|\mathbf{p} - \mathbf{p}_1\|. \quad (1a)$$

$$\Delta_k^o \stackrel{\text{def}}{=} d_k^o - d_1^o = \|\mathbf{p}^o - \mathbf{p}_k\| - \|\mathbf{p}^o - \mathbf{p}_1\|. \quad (1b)$$

Note that  $\Delta_k^o$  is fully known, while  $\Delta_k$  is unknown as it contains the (unknown) blind node position  $\mathbf{p}$ . Considering two packets  $i$  and  $j$  transmitted, respectively, by the blind and pivot node, their transmission and reception times are linked by the following equations ( $k = 1, \dots, K$ ):

$$r_{i,k}^* = t_i^* + \frac{d_k}{c} \quad (2a)$$

$$r_{j,k}^o = t_j^o + \frac{d_k^o}{c}. \quad (2b)$$

The relation between the reception time  $r_{i,k}$  and the associated timestamp  $s_{i,k}$  can be modelled as follows:

$$s_{i,k}^* = \alpha_k + (1 + \beta_k)r_{i,k}^* + h_k(r_{i,k}^*) + \omega_{i,k}^* \quad (3a)$$

$$s_{j,k}^o = \alpha_k + (1 + \beta_k)r_{j,k}^o + h_k(r_{j,k}^o) + \omega_{j,k}^o \quad (3b)$$

wherein

- $\alpha_k$  denotes the (unknown) initial temporal offset of node  $k$  clock with respect to the ideal time reference.
- $\beta_k$  denotes the (unknown) value of the *relative* frequency deviation of node  $k$  clock oscillator with respect to its nominal frequency. It is a dimensionless quantity that can take positive or negative values, normally limited to a few ppm. For a generic anchor, the value of  $\beta_k$  can be considered constant at the time-scales of interest for our problem (a few seconds or fractions thereof). Therefore, we obtain a trend component in the clock error that is linear in time and varies from anchor to anchor.
- $h_k(\tau)$  represents a *slowly-varying* function of time  $\tau$  that captures any non-stationary component of clock error (e.g. fluctuations of frequency offset due to temperature variations).
- $\omega_{i,k}^*$  and  $\omega_{j,k}^o$  represent the residual *fast-varying* error components. They absorb all non-systematic error components—e.g., random delays in the receiver processing chain, timestamp quantisation or truncation error, etc.—and can be modelled as independent random variables with general distribution, not necessarily zero-mean.

### 2.3. Algorithm overview

In the reference scenario outlined above, the only measurable quantities are the receiver timestamps collected by anchors. This is the input to the algorithm, along with the positions of all anchors and pivot nodes, i.e.,  $\{\mathbf{p}^o, \mathbf{p}_k, k = 1, \dots, K\}$ . The desired output is (an estimate of) the blind position  $\mathbf{p}$ . The localisation procedure is split into two stages, as depicted in Fig. 3, with a set of (differential) range measurements playing the role of intermediate variables. In the first stage, a set of differential ranges  $\{\Delta_k^*, k = 2, \dots, K\}$ —one for every quadruplet—is computed based on the input timestamps and node locations. In the second stage, the set of differential ranges is used to compute the final blind position.

In the first (differential) ranging phase we must cope with two types of unknown quantities: the blind node position,

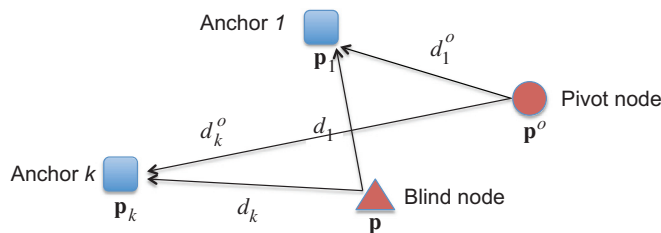


Fig. 2. Example of node quadruplet.  $K - 1$  total quadruplets are formed by considering different anchors  $k \in \{2, \dots, K\}$ .

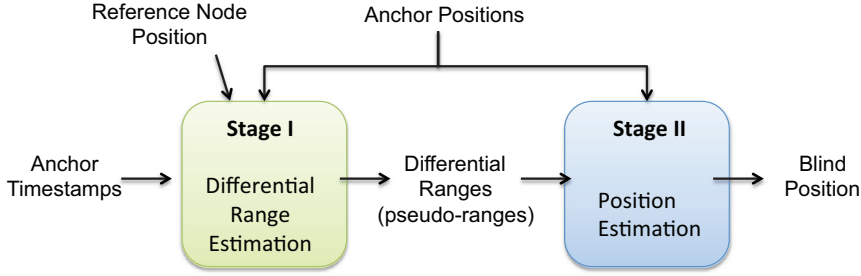


Fig. 3. Flow diagram of the proposed localisation procedure.

and various error components for each anchor clock. In order to produce differential ranges with acceptable accuracy we need to eliminate, or at least reduce, the systematic clock error components embedded in the raw timestamps. In our algorithm this is achieved through subtraction and rescaling of timestamps, as explained hereafter.

#### 2.4. Estimation of inter-anchor clock frequency ratio

In the first step we run a simple linear regression over a block of  $M$  data points  $\{s_{j,k}^o, s_{j,1}^o\}_{j=1\dots M}$ , i.e., pairs of reception timestamps collected at anchor  $k$  and at the reference anchor for a block of  $M$  consecutive packets transmitted by the pivot node—note that using the packets transmitted by the blind node  $\{s_{i,k}^*, s_{i,1}^*\}_i$  would be just equivalent. The slope factor of the regressed line, hereafter denoted by  $\hat{\gamma}_k$ , provides an estimate of the ratio between the *actual* clock frequencies of the two anchors, i.e.  $\hat{\gamma}_k \approx \gamma_k \stackrel{\text{def}}{=} \frac{1+\beta_1}{1+\beta_k}$  for  $k = 2 \dots K$ . This value will be used later to correct the timestamp measurements collected at anchor  $k$  before subtraction of the corresponding timestamps at the reference anchor, as explained below.

#### 2.5. Timestamp subtraction

Consider a pair of neighbouring packets  $i$  and  $j$  transmitted respectively by the blind node and by the pivot node in close by instants, e.g., one data packet and the corresponding acknowledgment. For these two packets, we consider a pair of receiving anchors: the reference anchor (for which  $k = 1$ ) and another generic anchor  $k \in \{2, \dots, K\}$ , as sketched in Fig. 2. Recalling (2) and (3) we can write:

$$s_{j,1}^o - s_{i,1}^* = (1 + \beta_1) \cdot (r_{j,1}^o - r_{i,1}^*) + n_{ij,1} \quad (4)$$

wherein for a generic anchor  $k = 1 \dots K$  (including the reference anchor) the error term

$$n_{ij,k} \stackrel{\text{def}}{=} \omega_{j,k}^o - \omega_{i,k}^* + h_k(r_{j,k}^o) - h_k(r_{i,k}^*)$$

cumulates the two individual random terms and the residual difference between the non-stationary error components. The latter is small, due to the fact that the reception times are close by and the function  $h_k(\tau)$  is slowly varying, formally:  $r_{j,k}^o \approx r_{i,k}^* \Rightarrow h_k(r_{j,k}^o) - h_k(r_{i,k}^*) \approx 0$ . By symmetry, the term  $n_{ij,k}$  can be modelled as a zero-mean random variable even if the individual components  $\omega_{j,k}^o$  and  $\omega_{i,k}^*$  have non-zero mean, since by definition they are (independent) variables extracted by the same process at anchor  $k$ . In other words,  $n_{ij,k}$  represents a measurement noise term.

For the same packet pair  $(i, j)$  we obtain an equation similar to (4) for every other anchor  $k \geq 2$ :

$$s_{j,k}^o - s_{i,k}^* = (1 + \beta_k) \cdot (r_{j,k}^o - r_{i,k}^*) + n_{ij,k}$$

and by multiplying by  $\gamma_k$  we obtain:

$$\gamma_k \cdot (s_{j,k}^o - s_{i,k}^*) = (1 + \beta_1) \cdot (r_{j,k}^o - r_{i,k}^*) + \gamma_k \cdot n_{ij,k} \quad (5)$$

(note the change from  $\beta_k$  to  $\beta_1$  in the right-hand term). Taking the difference of (4) and (5) and recalling (1) and (2) we obtain:

$$S_{ij,k} = (1 + \beta_1) \cdot \frac{\Delta_k - \Delta_k^o}{c} + n'_{ij,k} \quad (6)$$

wherein

$$S_{ij,k} \stackrel{\text{def}}{=} s_{j,1}^o - s_{i,1}^* - \gamma_k \cdot (s_{j,k}^o - s_{i,k}^*) \quad (7)$$

is the compound double difference of timestamps adjusted for *relative* clock skew (by  $\gamma_k$  rescaling), and

$$n'_{ij,k} \stackrel{\text{def}}{=} n_{ij,1} - \gamma_k \cdot n_{ij,k}$$

is a compound noise term. By using the estimate  $\hat{\gamma}_k$  (obtained previously from linear regression) in place of  $\gamma_k$  in (7) we compute an approximation  $\hat{S}_{ij,k}$  of  $S_{ij,k}$ , formally:

$$\hat{S}_{ij,k} \stackrel{\text{def}}{=} s_{j,1}^o - s_{i,1}^* - \hat{\gamma}_k \cdot (s_{j,k}^o - s_{i,k}^*). \quad (8)$$

The approximation error on  $S_{ij,k}$  is also zero-mean and can be absorbed into a total noise term, i.e.,  $N_{ij,k} \stackrel{\text{def}}{=} n'_{ij,k} + \hat{S}_{ij,k} - S_{ij,k}$ . With these positions we finally obtain:

$$\hat{S}_{ij,k} = (1 + \beta_1) \cdot \frac{\Delta_k - \Delta_k^o}{c} + N_{ij,k} \quad (9)$$

Fig. 4 reports the empirical distribution of the compound noise term  $N_{ij,k}$  expressed in ticks of 22 MHz clock. Each tick corresponds in space to  $\frac{22 \cdot 10^6}{3 \cdot 10^8} = 13.6$  m. The measurements were obtained from (9) in a symmetric squared topology, with the four nodes arranged in a way to ensure  $\Delta_k = \Delta_k^o \Rightarrow \hat{S}_{ij,k} = N_{ij,k}$ . It can be seen that the compound noise term has a zero-mean bell-like distribution. Although the initial measurement error on each individual data point may seem quite large, up to 30 m, the composition of multiple data points in time (by averaging multiple measurements for the same quadruplet) and space (by fusing measurements from different quadruplets) will drive the final position error down to metre level.

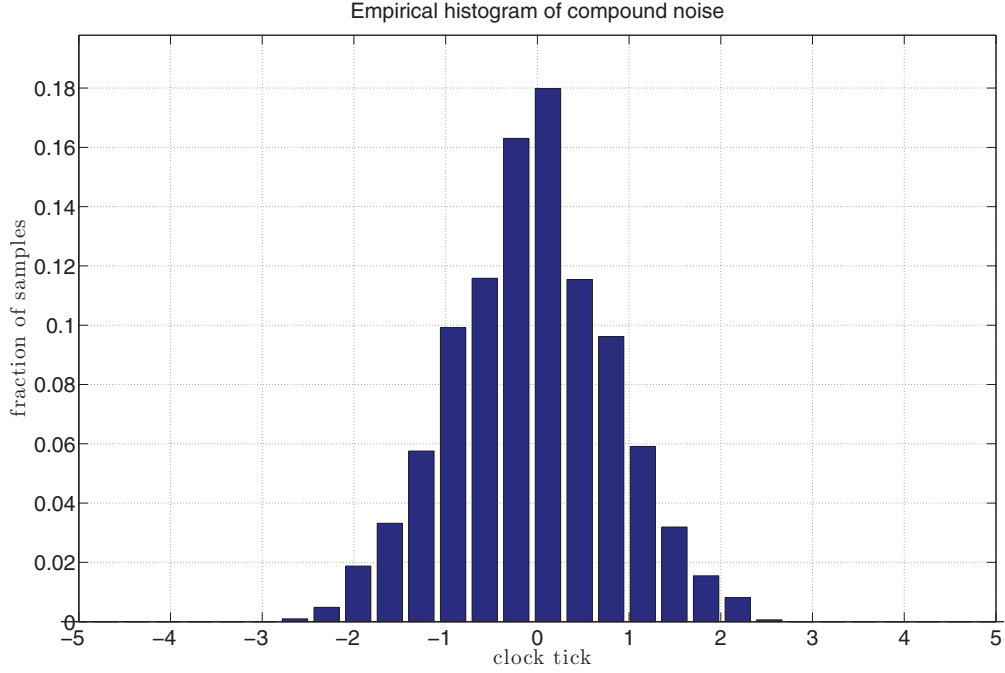


Fig. 4. Empirical distribution of compound measurement noise  $N_{ij,k}$  for one sample experiment.

2.6. Averaging and differential range computation

In our experiments the packets transmitted by the blind and pivot nodes alternate, so that at every receiver each packet from the blind node can be univocally associated with the successive packet from the pivot. Therefore, we can omit the index  $j$  and label exclusively by  $i$  (instead of  $ij$ ) the individual measurement originated by the generic packet pair. Furthermore, we set  $\mu \stackrel{\text{def}}{=} (1 + \beta_1)^{-1}$ . With these notational simplifications (9) rewrites as:

$$\mu \cdot \hat{S}_{i,k} = \frac{\Delta_k - \Delta_k^o}{c} + N_{i,k}. \tag{10}$$

wherein the scalar term  $\mu \approx 1$  accounts for the (unknown) frequency offset between the reference anchor and an absolute ideal clock. Recall that rescaling by  $\hat{\gamma}_k$  in (8) has compensated for the differences in frequency offset between the anchor nodes, thus aligning the whole system to a single common clock frequency (specifically the one of the reference anchor) but has not eliminated the absolute frequency offset of the system with respect to an ideal absolute clock. In other words, the effect of correcting for the relative frequency offset between the anchors emulates a system running with a single common clock affected by an unknown (small, but non-zero) skew term captured by  $\mu$ . As we will show later, the position estimation process is practically insensitive to a small common skew term, meaning that the approximation  $\mu = 1$  will introduce a negligible error on the final position (see proof in Appendix A).

In order to reduce the noise power, we average (10) over multiple packet pairs. Let  $\bar{S}_k \stackrel{\text{def}}{=} \frac{1}{M} \sum_{i=1}^M \hat{S}_{i,k}$  denote the average value of  $\hat{S}_{i,k}$  over  $M$  packet pairs, and  $\bar{N}_k \stackrel{\text{def}}{=} \frac{1}{M} \sum_{i=1}^M N_{i,k}$  the resulting average measurement noise. With these posi-

tions we finally obtain:

$$\Delta_k = \Delta_k^o + \mu \cdot c \cdot \bar{S}_k + c \cdot \bar{N}_k. \tag{11}$$

2.7. Position estimation

The output of the previous phase is a set of  $K - 1$  estimates of differential ranges  $\{\Delta_k, k = 2 \dots K\}$  between the blind node and each anchor pair  $(1, k)$  affected by (unknown) errors  $\bar{N}_k$ . The following positioning phase (ref. Fig. 3) takes in input the set of (estimated) differential ranges and the (known) anchor positions in order to finally estimate of the blind node position.

The position estimation problem can be casted into a least square (LS) optimisation problem.<sup>2</sup> Recall that the LS solution coincides with the maximum likelihood (ML) solution if the measurement noise is normally distributed—from Fig. 4 this assumption appears to be reasonable for our dataset.

The goal is to determine the blind node position  $\mathbf{p}$  that minimises the two-norm of the difference between the  $K - 1$  observations (one for each quadruplet) and the model (11), i.e., to compute:

$$\begin{aligned} \arg \min_{\mathbf{p}} \sum_{k=2}^K (\Delta_k - \Delta_k^o - \mu \cdot c \cdot \bar{S}_k)^2 \\ = \arg \min_{\mathbf{p}} \sum_{k=2}^K (\|\mathbf{p} - \mathbf{p}_k\| - \|\mathbf{p} - \mathbf{p}_1\| - \Delta_k^o - \mu \cdot c \cdot \bar{S}_k)^2. \end{aligned} \tag{12}$$

<sup>2</sup> Note that the error terms  $\bar{N}_k$  are not independent, i.e., their covariance matrix is not diagonal. However, for the sake of simplicity, we neglect here correlations between the error terms and consider an ordinary (non-weighted) least square estimation approach.

The actual value of  $\mu \stackrel{\text{def}}{=} (1 + \beta_1)^{-1}$  is unknown, but we can safely neglect it, since the relative error caused by the approximation  $\mu \approx 1$  on the final position estimate is negligible, comparable with the value of  $|\beta_1|$ —typically in the order of  $10^{-5}$  (see proof in Appendix A). With this simplification the estimation problem rewrites as:

$$\arg \min_{\mathbf{p}} \sum_{k=2}^K (\|\mathbf{p} - \mathbf{p}_k\| - \|\mathbf{p} - \mathbf{p}_1\| - \Delta_k^o - c \cdot \bar{S}_k)^2. \quad (13)$$

This is a non-linear minimisation problem to be solved numerically. We consider two different resolution methods, hereafter denoted as “HYP” and “ILS”. Both methods follow the same high-level approach based on the iterative resolution of (a sequence of) problem instances representing linearised version of (13). However, they differ in the details of how linearisation is achieved.

**Hyperbolic equations (HYP) on differential ranges.** This is the method described in [35], and specifically Eqs. (1)–(7) therein. The problem (13) is linearised directly via Taylor-series approximation. The name of the method is due to the fact that each term of the form  $\|\mathbf{p} - \mathbf{p}_k\| - \|\mathbf{p} - \mathbf{p}_1\| = \text{constant}$  describes an hyperbola with foci in  $\mathbf{p}_k$  and  $\mathbf{p}_1$ .

**Iterative least squares (ILS) on pseudo-ranges.** This is the standard positioning algorithm adopted in GPS (see e.g. [36]) based on an iterative least squares (ILS) procedure run on a set of *pseudo-ranges* between the blind node and a set of reference points in known positions (satellites in GPS). The term “pseudo-ranges” denotes a set of ranges, i.e., distances, determined up to an additive common bias term, formally  $\{d_k^* + \delta, k = 1, \dots, K\}$  where  $\delta$  plays the role of an additional variable in the estimation problem. The ILS algorithm, which was successfully used in a similar context also in [33,34], is able to jointly determine the blind position and resolve for  $\delta$ . In order to apply ILS, we need first to transform the range of differential ranges  $\{\Delta_k, k = 2, \dots, K\}$  into a set of pseudo-ranges. This is achieved by a simple variable substitution  $d_1^* = \delta$ , i.e., letting the distance between the blind node and the reference anchor be treated as an additional independent variable  $\delta$ . In this way, the set of remaining distance variables take the form of a set of pseudo-ranges, i.e.  $\{d_k^* = \Delta_k + \delta, k = 2, \dots, K\}$ . With the variable substitution  $d_1^* \stackrel{\text{def}}{=} \|\mathbf{p} - \mathbf{p}_1\| = \delta$  the problem (13) is first transformed into the following alternative formulation:

$$\arg \min_{\delta, \mathbf{p}} \sum_{k=2}^K (\|\mathbf{p} - \mathbf{p}_k\| - \delta - \Delta_k^o - c \cdot \bar{S}_k)^2 \quad (14)$$

then linearised and solved iteratively.

Both HYP and ILS algorithms start from a rough initial guess and improve iteratively at each step by determining the local linear least-sum-squared-error correction. In our implementation the starting point is set to the centre point between all anchors.

### 3. Experimental results

The main challenge is to capture into the model, and properly correct in the algorithm, the non-idealities of the

real timestamping process in standard COTS receivers. For this reason it makes sense to validate directly our approach experimentally, with real measurements obtained from a testbed with COTS devices, instead of resorting to abstract simulations.

#### 3.1. Testbed setup

For our measurement testbed we use WRT54GL devices from Linksys. This choice was motivated by several reasons: (i) their price is very affordable, less than 40 USD on ebay; (ii) they run a very robust OpenWRT distribution based on Linux Kernel 2.6.32; (iii) their wireless Network Interface Card (NIC) is compatible with OpenFWWF [37], an open source firmware that replaces the original binary-only software from Broadcom and has been widely used as research platform [38–40]. The basic version of OpenFWWF implements a fully working distributed coordination function (DCF) and timestamps each incoming packet with the value of the Basic Service Set clock, sampled by the underlying hardware when a preamble is successfully received. Unfortunately this clock has only 1 MHz resolution. For this reason we modified the real-time receiving part of the code to spin during the reception of specific packets until they are completely decoded: right after the single instruction spinlock, a sample of the 32 bit internal clock that drives the execution pipeline is taken and reported to the Linux kernel. As a result, we obtain timestamps with clock frequency of 22 MHz, corresponding to a clock tick of 45.4 ns (13.6 m at speed light). These operations are executed only for UDP packets with configurable destination port which we check as soon as the first bytes of each frame are received.

Every node is programmed to transmit UDP packets with a payload of 10 bytes. Every packet is transmitted with a single attempt at the MAC layer in order to avoid ambiguities in correlating copies of the same packet received by different nodes. In a real scenario this is equivalent to consider only the first transmission of a frame (retry bit set to 0). The nodes schedule UDP packet transmissions with an inter-departure period of 10 ms at the application level. Then, at the MAC layer, the channel access is performed using the standard DCF protocol with a Contention Window of 15 slots. All nodes are set to transmit in IEEE 802.11g mode with DSSS modulation, transmission rate of 2 Mb/s and long preamble of 192 bits. Every node transmits at an average rate of about 92 packets/s. Every node logs the local reception timestamp, source address and packet identifier for each received packet. Depending on the role assigned to each node in each trial (blind, pivot or anchor) we disregard the packets transmitted or received by that node in that trial.

We conducted two distinct sets of experiments. In the first set, all nodes were in full line-of-sight (LOS) conditions and all transmissions took place on a single frequency channel (specifically, channel #1). We tested two different environments: outdoor (garden) and indoor (gym), as described below. In each scenario we have used seven nodes, thereof six (anchors and pivot) in fixed positions that did not change across the different experiments (squares in Fig. 5), and one (blind node) placed in a different position for each experiment. The actual node positions (ground truth) were measured manually with an accuracy in the order of 2–3 cm. A

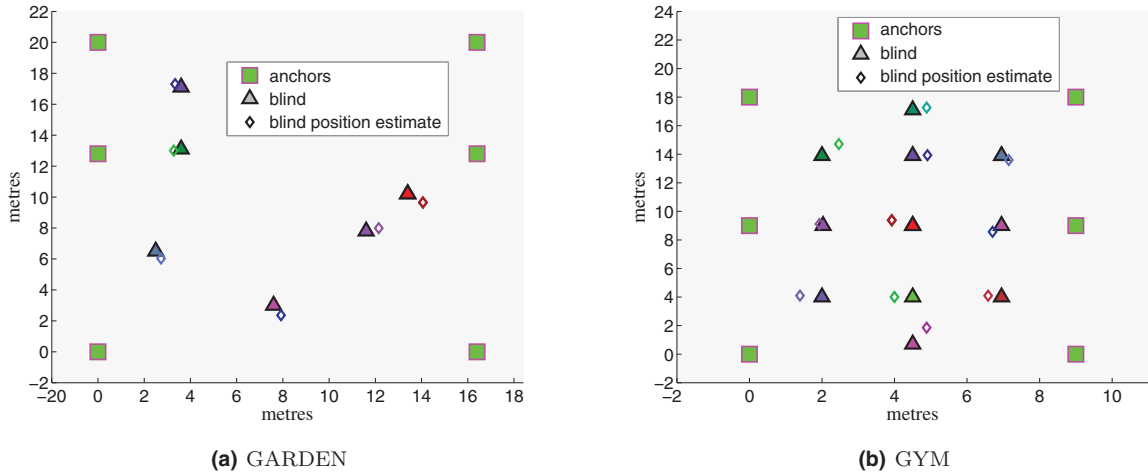


**Fig. 5.** Node locations during the experiments. In each scenario, six nodes were kept fixed at locations marked by squares. In each experiment, one node was moved to a different location among those indicated by triangles. The legend refers to the role of each node in the “active anchors” setting described in Section 4.

third set of experiments was conducted in mild non-line-of-sight (NLOS) conditions within the main university entrance hall. The testbed setting and results will be presented separately in Section 5.

#### First test scenario: GARDEN (full LOS)

The first set of experiments was conducted outdoor in a free area, i.e., a green garden. In this test all nodes are placed at 10 cm height from the ground within a rectangle of  $16 \times 20$  m (ref. Fig. 5(a)). All nodes are in line-of-sight, without any intermediate obstacle, and the only possible source of multipath error are reflections from the ground. Note that in this experiment each node was using two receiving antennas, as per the default configuration. We run 6 experiments with different positions of the blind node, indicated by triangles in Fig. 5(a).

#### Second test scenario: GYM (full LOS)

The second set of experiments were conducted in a large clear indoor area, i.e., a school gym. Nodes were placed at the height of 1.5 m from the ground within a rectangle of  $9 \times 18$  m (ref. Fig. 5(b)). Similarly to the previous test, all nodes are in line-of-sight, without intermediate obstacles, and the only possible sources of multipath error are reflections from the floor, from the ceiling and from the perimeter walls, the latter being located at an horizontal distance of 4–5 m from the nodes. Differently from the previous experiments, we removed one of the two antennas from each device in order to enforce single-antenna reception: in fact, if the receiver adopts phase-adjusted combination of the signal from different antennas (e.g. maximum ratio combination), this results in an implicit directionality of the receiving antenna patterns that could in principle increase the risk of reception over non-line-of-sight paths. In this scenario we run 11 experiments with different positions of the blind node (triangles in Fig. 5(b)).

### 3.2. Experimental results with single pivot

For each experiment, we run six different trials by assigning the role of pivot node to each of the fixed nodes, the remaining five playing the role of anchors. Therefore, we have a set of 36 different trials (i.e., different configurations of blind, pivot and anchor positions) for the GARDEN scenario and 66 for GYM. For each trial, we compute the estimated blind position with the algorithm under test, and from there the final position error, i.e., the distance between the estimated and true positions. In order to compare different variants of our method, we plot the empirical cumulative distribution function (ECDF) of the final position error.

Fig. 6(a) and (b) report the ECDF of the position error, respectively, for the two positioning methods HYP and ILS in the GARDEN scenario. Similarly, Fig. 6(c) and (d) compare HYP and ILS in the GYM scenario. The plots are obtained with a single block of  $M = 200$  packet pairs for each trial, corresponding to a measurement interval of approximately 2 s—recall the packet inter-departure time was set to 10 ms. For each positioning method we have tested three different strategies with respect to the choice of the reference anchor:

- **near:** choose as reference the nearest anchor to the pivot;
- **far:** choose the farthest anchor from the pivot;
- **mean:** run the algorithm  $K$  times, for all possible choices of reference anchor, and take the mean of the  $K$  points.

The plots in Fig. 6(a) and (c) show that the choice of the reference anchor has a certain impact on the final accuracy when HYP positioning is used, especially in the GYM dataset, and that it is always preferable to choose the nearest anchor to the pivot. The plots in Fig. 6(b) and (d) show instead that ILS positioning is pretty insensitive to the choice of reference anchor. Overall, ILS and HYP (with near-pivot reference anchor) yield comparable accuracy, with median error around 1–1.2 m and maximum error around 3 m. In the remaining of this paper we will use ILS with near-pivot reference anchor, unless differently specified.

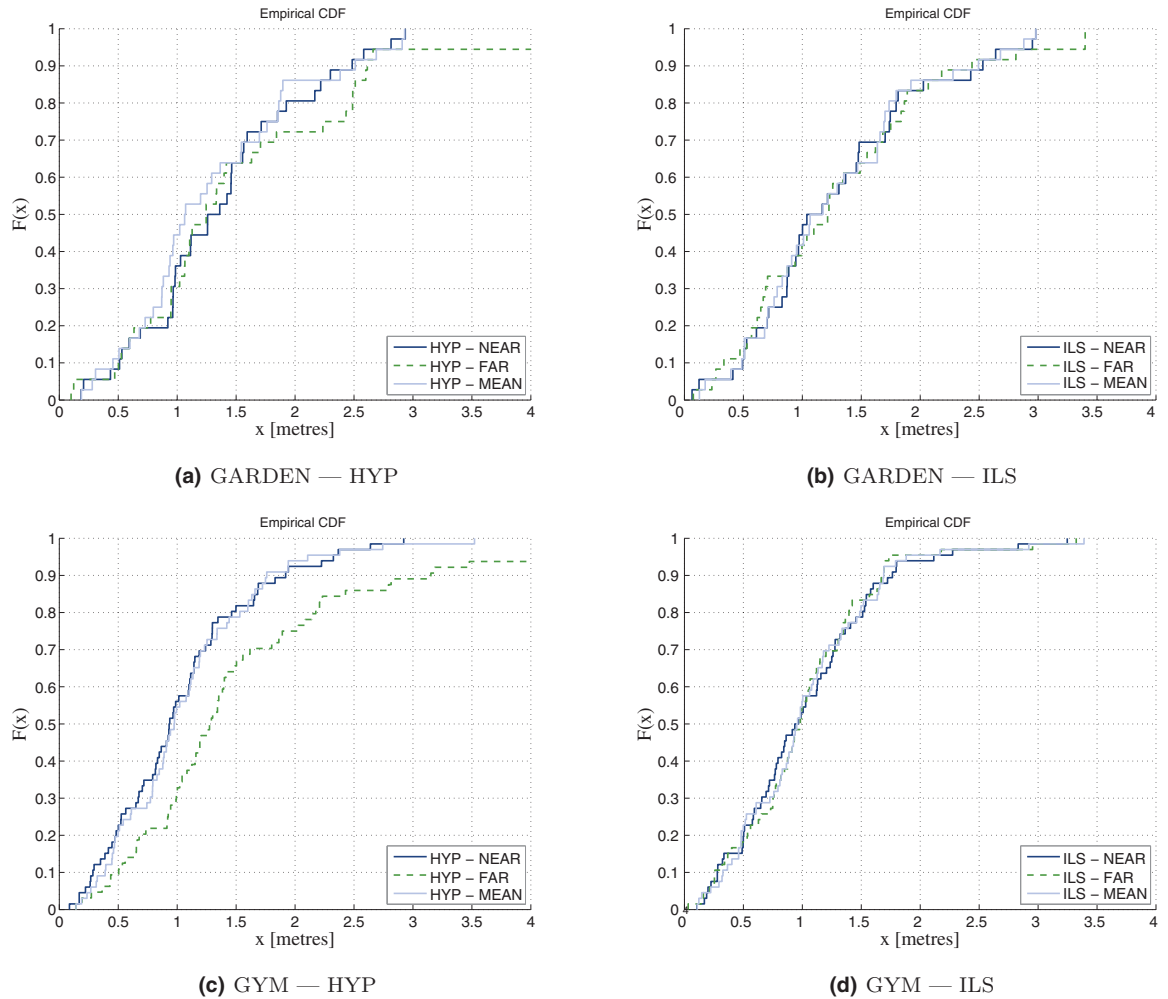


Fig. 6. Comparison between HYP (left column) and ILS positioning (right column), for different choices of reference anchors and  $M = 200$ .

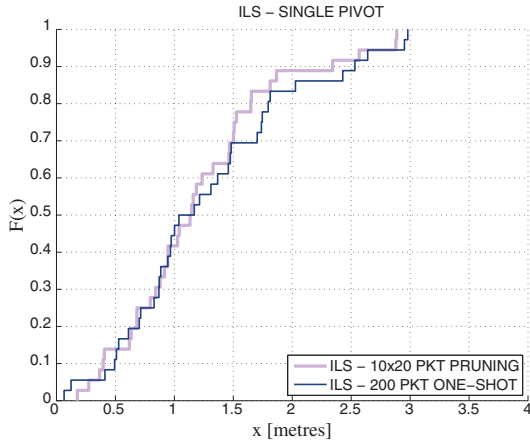
In the next test we are interested to compare two different strategies for combining different subsets of measurements. Considering a large dataset of (timestamps associated with)  $B$  packet pairs (e.g.  $B = 200$ ) collected at  $N$  anchors, for a total of  $N \cdot B$  timestamps, we consider the following strategies:

- **One-shot.** The localisation procedure described above is run once, with the whole set of measurements in input. In other words, all  $N \cdot B$  timestamps are processed jointly in a single block.
- **Slice & prune (S&P).** With this approach the set of available measurements is first “sliced” into  $L > 1$  smaller subsets, not necessarily disjoint, as explained below. The localisation procedure is run independently for each data subset, resulting in a set of  $L$  intermediate estimates (data points). An iterative pruning process is applied onto this set: take the mean  $\bar{\mathbf{p}}_L$  of all  $L$  data points and then prune out the single element point that is farthest from  $\bar{\mathbf{p}}_L$ , thus reducing to  $L - 1$  data points; re-compute the mean  $\bar{\mathbf{p}}_{L-1}$  and iterate the pruning procedure until the number of residual data points reaches a pre-determined stop value

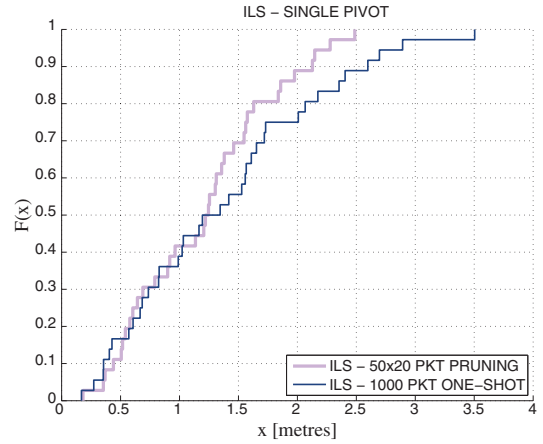
$L_{\min}$ ; the mean value  $\bar{\mathbf{p}}_{L_{\min}}$  of the residual points is then taken as the final estimate. In our implementation we set  $L_{\min} = L/2$ . This simple pruning procedure is meant to reject data points with occasionally high error, thus reducing automatically to a smaller subset of more consistent data points.

The initial slicing of input measurements can be performed across one or more of the following dimensions: time, space and frequency:

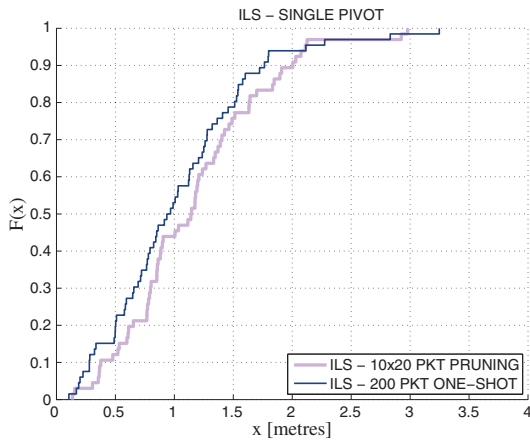
- **Temporal slicing:** a sequence of  $B$  packet pairs transmitted on the same channel at different times is sliced into  $M$  smaller blocks of  $B/M$  packet pairs each.
- **Spatial slicing:** from the set of  $N$  anchors we can select  $\binom{N}{n}$  subsets of  $n \leq N$  anchors. In order to compute a candidate position estimate, we need at least three anchors. Therefore, we consider all possible subsets of three or more anchors. The total number of such subsets is  $H_{N,3} = \sum_{n=3}^N \binom{N}{n}$ . For instance, with  $N = 6$  we have  $H = 42$  valid subsets.



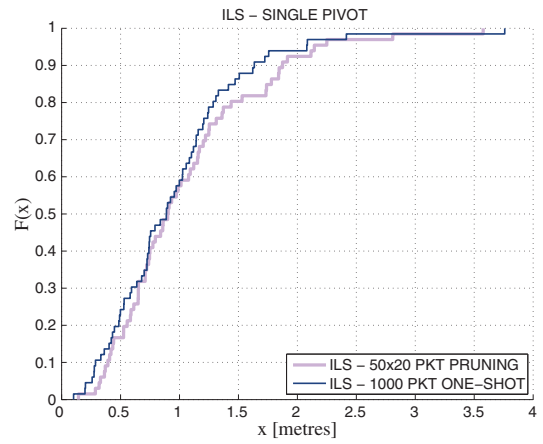
(a) GARDEN —  $B = 200$



(b) GARDEN —  $B = 1000$



(c) GYM —  $B = 200$



(d) GYM —  $B = 1000$

Fig. 7. Comparison “one-shot” versus “slice & prune” for  $B = 200$  and  $B = 1000$  (single channel measurements).

- **Frequency slicing:** if measurements are performed across multiple frequency channels, a natural way of slicing the input data in frequency is to divide them on a per-channel basis.

In the GARDEN and GYM experiments all measurements were collected on a single channel, therefore frequency slicing does not apply. For these two experiments we compared the one-shot strategy against the S&P with joint temporal/spatial slicing. In Fig. 7 we compare the ECDF of the final error obtained with these two strategies, for  $B = 200$  and  $B = 1000$ . For the pruning method we have set  $M = 20$ ,  $H = 42$ ,  $L = H \cdot M$  and  $L_{\min} = \frac{1}{2} \cdot L$ . The first observation is that the two methods yield comparable results for most of the trials. In the GARDEN experiments, the S&P method is able to reduce the error for the few trials with larger error (upper tail of the ECDF).

The second observation is that using more packets does not necessarily lead to better accuracy: comparing the plots for  $B = 200$  and  $B = 1000$  it can be seen that the accuracy remains substantially unchanged with S&P, and slightly de-

grades with the one-shot method for the GARDEN experiment (note the rightward drift of the upper tail of ECDF). The latter finding indicates that the timestamp measurements collected in the testbed are not only affected by a random component, i.e. measurement noise, which in general can be reduced by increasing the number of observations (i.e., packets) but also embed some form of *systematic* bias accountable to multipath.

#### 4. Extension to active anchors

Until now we have considered a system model with a single transmit-only pivot and multiple receive-only (passive) anchors, as sketched in Fig. 1(a). One obvious extension is to consider a system with *active anchors*, i.e., where all infrastructure nodes are capable of both transmitting and receiving (and therefore timestamping) the packets or beacons from other anchors and from the blind node. This new scenario, sketched in Fig. 1(b), will become more and more relevant for practical applications as new systems are emerging that

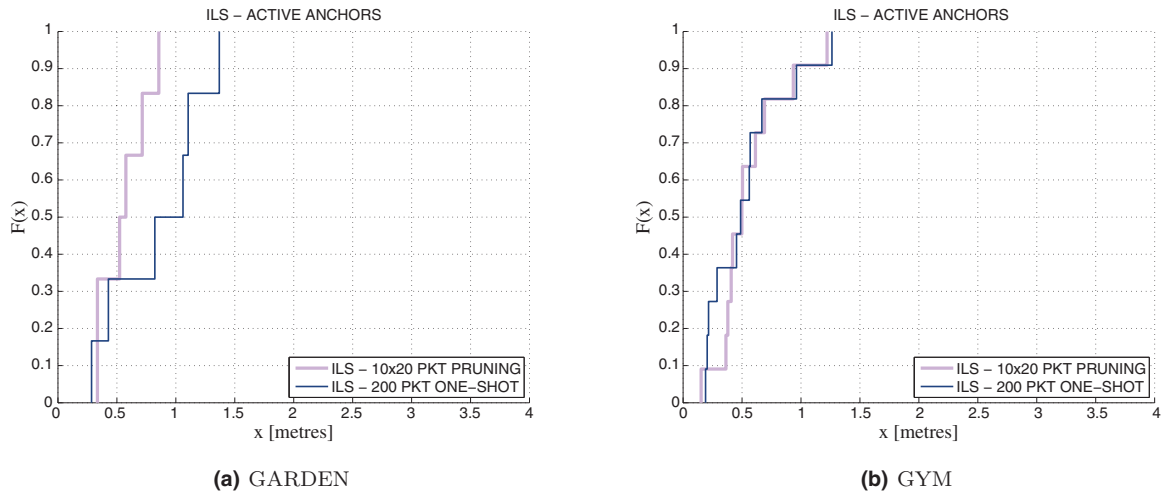


Fig. 8. Distribution of absolute positioning errors with active anchors. For each experiment the corresponding blind position estimates are plotted in Fig. 5.

involve dense deployments of many low-cost infrastructure nodes, e.g. based on Bluetooth Low-Energy technology [41] and in WSN applications.

It is straightforward to adapt our algorithm to work in the active anchors scenario. The signal reference function, that in the previous scenario was performed by the pivot node, can be now absorbed by the anchor themselves: timestamp adjustment will rely on anchor-to-anchor communications, instead of pivot-to-anchors. It is reasonable to expect that the active anchors scenario will allow for higher estimation accuracy when compared with the single-pivot method for the same number and placement of infrastructure nodes, due to the higher *volume* of available data (i.e., transmitted packets, hence timestamps) and *diversity* of transmitting positions.

We seek to extend the algorithm presented in the previous section to address the active anchors scenario without adding too much implementation complexity. Motivated by the positive results obtained in the previous experiments we resort to a procedure based on the same “slice & prune” principle described above. The key idea is to consider a single scenario with  $N$  active anchors as the overlay of  $N$  parallel sub-scenarios, each with 1 transmit-only pivot and  $N - 1$  receive-only anchors. In other words, we are “slicing” the problem instance into  $N$  parallel instances—not completely disjoint, as the packets transmitted by the blind node will be common to all sub-instances. Each of the  $N$  sub-instances can be further sliced in space—considering all subsets of three or more anchors, resulting in  $H_{N-1,3} = \sum_{n=3}^N \binom{N-1}{n}$  slices—and in time—dividing the block of  $B$  packets in  $M$  sub-blocks. By running the basic positioning procedure for each slice of each sub-instance, we produce a set of  $L = N \cdot H_{N-1,3} \cdot \frac{B}{M}$  data points, each produced by a different set of input data. The last step is to apply the iterative pruning procedure described above and take the mean value of the residual  $L_{\min}$  data points as the final position estimate.

As done above, we compare this S&P approach versus a more compact method, where a single datapoint is obtained

for each sub-instance by using all  $B \cdot (N - 1)$  timestamps without slicing, and the mean value of the  $N$  data points is taken directly as final estimate (no iterative pruning). For each experiment (6 in GARDEN scenario and 11 in GYM) we run the two methods on the same sample dataset, considering the first  $B = 200$  packets transmitted by each node in the given experiment. The final absolute error CDF is reported in Fig. 8. Consistently with what was observed in the previous test, the S&P method helps to reduce the final errors in GARDEN (the maximum error reduced from 1.8 to 0.8 m), while in GYM it has no evident influence on the accuracy. The final positions estimated with the S&P method for each experiment are also reported as diamond markers in Fig. 5. The median error is around 0.5 m in both environments, and the maximum error is 0.8 m and 1.3 respectively in GARDEN and GYM.

## 5. Robustness to mild NLOS conditions

The results presented above are quite remarkable considering that we have used relatively affordable COTS devices without putting in place any synchronisation mechanism. However, they were obtained in full LOS conditions, i.e., all nodes (anchors and blind) were in direct visibility to each other. In order to explore the impact of NLOS on the final accuracy of the proposed method, we conducted an additional series of experiments (“HALL”) in a more complex indoor environment, at the main entrance hall of the university building.

For this new set of experiments we used a total of 10 nodes (nine active anchors plus one blind node) arranged in six different topologies. Seven anchors were deployed in the main entrance hall while the remaining two anchors were positioned in nearby corridors, without direct visibility to all other nodes. Note that all node pairs could successfully exchange packets, i.e., NLOS links were not in outage. This resulted in a mixture of LOS and NLOS links, with prevalence of LOS links. In other words, we reproduced “mild NLOS” conditions according to the taxonomy proposed in [42]. To

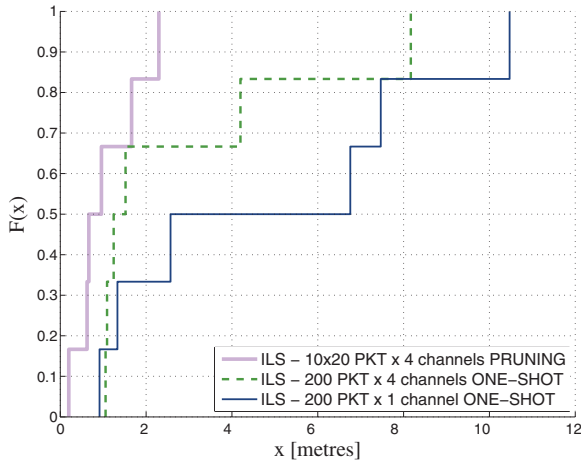


Fig. 9. Distribution of absolute positioning errors for HALL experiments (six trials) in mild NLOS conditions.

counteract the NLOS error we leveraged *frequency diversity*: different blocks of packets were transmitted on four different radio channels—specifically channels #1, #5, #10 and #14 of IEEE 802.11g—and frequency slicing was adopted along with temporal and spatial slicing in S&P.

The results are reported in Fig. 9. The rightmost curve shows the final error obtained by the one-shot estimation with data from a single channel. This curve should be compared with the one-shot curves in Fig. 8 that were obtained in similar setting (block of  $B = 200$  packet pairs transmitted on single-channel and processed in one-shot), the only difference being (i) the number of anchors and (ii) the presence of NLOS link. Despite the HALL experiments were performed with more anchors than GYM and GARDEN (nine against seven), the one-shot approach cannot prevent the final positioning error to increase dramatically, due to NLOS error in input: the worst case error rises from less than 1.5 m in GYM/GARDEN (ref. Fig. 8) to more than 10 m in HALL. The middle curve in Fig. 9 was obtained with multi-channel measurements over 4 different channels, for a total of  $4 \cdot B = 800$  packet pairs, processed together in a single round. Compared with the previous curve, it can be seen that the introduction of frequency diversity (multi-channel measurements) has a limited positive impact on the final error—the maximum value reduces to 8 m.

The leftmost curve was obtained by running the S&P algorithm on multi-channel data. Slicing was applied over all three dimensions—time, space and frequency. The coupling of S&P and frequency diversity leads to a dramatic improvement, with a reduction of the maximum error down to 2 m, and a median error of only 1 m, not much higher than what was obtained in GYM and GARDEN in full LOS conditions. These three curves demonstrate two things. First, that the basic DTDoA with one-shot estimation is extremely sensitive to NLOS, and even a small amount of NLOS links has devastating effect on the final accuracy. Second, that combination of S&P and multi-channel measurements is successful in rejecting (a limited amount of) input NLOS errors, enabling the practical adoption of DTDoA in mixed LOS/NLOS environments.

## 6. Discussion and outlook on future work

### 6.1. Improving robustness in heavy NLOS scenario

In practical settings the most serious source of error is NLOS propagation. Following [42] we discriminate between “mild NLOS” and “heavy NLOS” environments, depending on whether the LOS links are prevalent or not. Our experimental results were obtained in full LOS (GYM and GARDEN experiments) or mild NLOS conditions (HALL experiments). In the latter case, we managed to maintain satisfactory results by leveraging frequency diversity—in addition to spatial and temporal diversity—via the S&P method with multi-channel measurements. We remark that the S&P method plays a key role in rejecting a small amount of NLOS error (recall from Fig. 9 that simple averaging over multiple channels does not achieve the same improvement). However, our method will simply not work satisfactorily in heavy NLOS environments.

Generally speaking, the NLOS problem affects all radio localisation methods, whether RSSI-based or time-based, including the traditional ToA, TDoA and of course also the DTDoA method considered here. In other words, it should not be considered as problem specific to our method. However, NLOS errors propagate in different ways within ToA, TDoA and DTDoA localisation procedures. Therefore, the great deal of proposed solutions for NLOS mitigation that have been developed for ToA and TDoA (see [42–44] and references therein) will probably need careful adaptation before they can be applied to DTDoA systems. For this reason, further work is needed to understand the sensitivity of DTDoA to NLOS errors and to develop NLOS mitigation strategies specifically for DTDoA. One important direction in this regard, is to leverage physical layer information, from simple RSSI up to channel state information (CSI) and angle-of-arrival (AoA) as done e.g. in [45] with IEEE 802.11n nodes. However, this approach comes at the cost of reduced generality, as it imposes additional requirements on the transceiver devices (e.g. multiple antennas with synchronous receiver chains, and firmware support for CSI exporting) and implicitly rely on specific radio standard (e.g. IEEE 802.11n). In other words, exploiting PHY information involves a trade-off in the applicability space: it widens the range of environments where time-based localisation can be satisfactorily adopted (from pure LOS and mild NLOS environments towards heavy NLOS spaces), at the cost of shrinking the range of transceiver models and radio standards that can be used for this purpose.

### 6.2. Distributed and secure computation

In this work we have considered a centralised approach, where a single entity (e.g., a localisation server or cloud service) concentrates all the data and computation. However, owing to the fact that the basic algorithm involves simple linear operations, it should be possible to devise methods to perform the same computation in a distributed fashion, without the need of data centralisation. Another related research direction would be to explore the possibility of performing the localisation procedure without revealing some of the input data, that might be considered sensitive

by the participating entities, e.g., the (known but private) anchor node positions, by drawing methods from the field of privacy-preserving computation and secure multiparty computation.

## 7. Related work

The vast majority of previous work on time-based localisation in asynchronous networks (e.g. [18–24]) rely on the knowledge or tight control of transmission times (in addition to reception times) and anyway require some form of involvement by the blind node. For these reasons, such methods cannot be used to implement fully opportunistic localisation on top of legacy wireless systems with COTS hardware, and therefore cannot be directly compared to our work.

The method elaborated in this paper relies on the (double) subtraction of four arrival times referred to a quadruplet of nodes—two transmitting and two receiving, ref. Eq. (6)—in order to get rid of the unknown transmission times and clock offsets. This basic principle characterises an entire class of techniques that are commonly referred to as differential time-difference of arrival (DTDoA)—to distinguish from the classical ToA and TDoA approaches that require synchronisation between all nodes (ToA) or between the anchors (TDoA). Considering the relative ease of adoption and the possibility to “opportunistically” implement DTDoA in legacy systems, it is a bit surprising that DTDoA techniques have attracted very small attention by the wireless networking community until now, at least when compared to the much more popular TDoA methods that, conversely, require to put in place additional burdensome synchronisation mechanisms. In this section we review previous work on DTDoA methods and their experimental evaluation, highlighting the main differences with our work.

The DTDoA principle is reminiscent of the “double-difference” method applied in GNSS to eliminate residual errors on the carrier *phase* for high-precision applications (see e.g. [27]). Considering the problem of terrestrial (non GNSS) localisation with time (not phase) measurement, the DTDoA principle first appeared a decade ago in the context of interferometry [28] and was later considered in systems where the time difference between two terrestrial signals from distinct transmitters is measured by waveform correlators [29,32,46,47]. This approach demands specialised processing at the physical layer and/or considerable additional capacity to exchange sampled waveforms between the nodes, therefore cannot be implemented on top of legacy devices and systems. The idea of using simple reception timestamps (as opposite to cross-correlation and interferometric measurements) in a DTDoA context was considered in [30,31]. The work in [30] addresses the problem of localising a set of *receivers* (from legacy TV and AM broadcast signals), while here we focus on the opposite problem of localising a *transmitter* (of WiFi or other packet-based protocol).

The recent work [31] is certainly the closest one to our work: the system model considered therein is equivalent to our single-pivot scenario, and the localisation procedure described there is similar to the basic scheme proposed here with passive anchor. However, there are a number of differ-

ences between the two methods. First, we obtain (an estimate of) the relative clock skews (factor  $\gamma_k$ ) by linear regression over a block of multiple packets, instead of subtraction between consecutive packets and filtering as done in [31]. This allows for a more robust and simple estimation. Second, we adopt ILS positioning instead of hyperbolic equations, which (as we have shown) delivers slightly more stable results. Third, we combine the basic method with a novel “slice & prune” strategy that, on one hand, adds robustness by rejecting occasional “bad” data and, on the other hand, provides a very simple approach to effectively fuse data from different transmitters (pivot nodes) if available. In this way, it is straightforward to apply our localisation procedure to the active anchors scenario, which was not considered in [31] and whose relevance for practical applications is probably going to increase in the near future, following the widespread of wireless systems with dense deployment of low-cost fixed nodes, e.g. based on Low-Energy Bluetooth [41] and in WSN. Note also that the experimental results reported by [31] are limited to 1D localisation, i.e., the blind node is constrained on a linear axis, while in our experiments we consider 2D localisation. Finally, it should be mentioned that the testbed results reported in [31] were obtained with a self-developed transceiver device rather than COTS hardware. To the best of our knowledge, the present paper is the only work to report sub-metre accuracy for 2D localisation from experimental measurements obtained exclusively with unsynchronised COTS devices.

For the sake of completeness we cite also the work by Coluccia et al. in [33] and [34] where the problem of time-based localisation in asynchronous networks is addressed from a slightly different perspective. While DTDoA methods eliminate both unknowns, namely the transmission time and the clock bias, by *double subtraction* between four link equations for a *quadruplet* of nodes (two transmitters and two receivers), Coluccia et al. resort to *single subtraction* between two link equations for a *triplet* of nodes, namely two transmitters and one receiver [33], or one transmitter and two receivers [34]. In this way, they eliminate only one of the two unknowns—namely the clock bias in [33] and the transmission time in [34]—and treat the other unknown as a nuisance parameter to be estimated jointly with the (pseudo)-ranges. However they do not consider clock drifts in their model: this is a serious limitation for the applicability of their methods in practical scenarios where clock frequency deviations cannot be ignored—in fact [33,34] provide only simulation results, not experimental validation. We believe however that future extensions of those works in the direction of a more realistic clock error model bear the potential to improve further the achievable localisation and possibly beat our method.

## 8. Conclusions

We have proposed and demonstrated a radio-based localisation method that relies exclusively on the reception timestamps collected by multiple anchors for the packets transmitted by the blind node and (at least one) other emitting node(s) in known position(s). Differently from traditional time-based localisation schemes, our method does not require any form of node synchronisation, nor the

measurement (or control) of transmission timestamps. Also, it does not require the collaboration of the blind node, that can be localised while performing standard communication functions. The proposed method can be run “opportunistically” on legacy signals and packets transmitted over-the-air for communication purposes, regardless of the signal format and protocol, and in principle can be applied to any wireless technology (including WiFi, Bluetooth, IEEE 802.15.4, DVB-T, UMTS, LTE, etc.) and any combination thereof.

In principle, the system model can be applied to “cooperative localisation” scenarios where some of the (transmitting and/or receiving) mobile nodes know their position only approximately, e.g., from their onboard GNSS module. These nodes can participate to the localisation procedure by providing timestamp measurements (as receivers) and/or reference signals or packets (as transmitters), similarly to the scenario considered already in [33]. The (unknown) error in the initial position of these nodes represents an additional source of measurement error that, however, does not break the conceptual formulation of the problem. The joint processing of these data (initial positions and reception timestamps) not only provides a position estimate for the blind node(s), but bears also the potential of improving the initial position estimate delivered by GNSS modules. In other words, it can serve as a “cooperative augmentation” strategy for GNSS positioning that, differently from previous proposals [48,49], does not require the implementation of additional ranging functions and sensors but can exploit opportunistically existing communication signals and devices.

The experimental results presented in this work indicate that sub-metre accuracy can be reached nowadays with low-cost COTS hardware, at least in LOS conditions. We believe that the combination of minimal implementation requirements and good achievable accuracy make this approach very appealing for practical applications in a wide range of application scenarios, most prominently those characterised by a high density of radio devices and signals, e.g., for indoor positioning in crowded areas (stations, airports, shopping centres) and in C-ITS applications.

In the progress of the work we aim at exploring more advanced estimation methods for the problem at hand that can be naturally extended to cope with mobile nodes (blind and/or anchors), thus shifting the focus from the problem of static positioning towards dynamic tracking. Another important direction for further work is to develop robust NLOS mitigation strategies tailored for the scenario at hand.

### Additional resources

The experimental datasets and all the software developed to setup the testbed are available for non-anonymous download from <http://www.ing.unibs.it/~openfwwf/localisation>.

### Acknowledgements

The work by F. Gringoli and N. Facchi was partly supported by the European Union under projects FP7-258301 (CREW) and H2020-645274 (WiSHFUL). F. Ricciato would like to thank Dr. Reinhard Exel for some fruitful discussions about the impact and mitigation of NLOS in DTDoA scenarios.

## Appendix A. Proof of insensitivity to a common skew term

Hereafter we proof that fixing  $\mu \stackrel{\text{def}}{=} (1 + \beta_1)^{-1} \approx 1$  in the position estimation problem (12) leads to an error (in metres) comparable to  $|\beta_1| \ll 1$ , whose typical values are in the order of few ppm. In fact (12) can be rewritten as:

$$\begin{aligned} & \arg \min_{\mathbf{p}} \sum_{k=2}^K (\|\mathbf{p} - \mathbf{p}_k\| - \|\mathbf{p} + \mathbf{p}_1\| - \|\mathbf{p}^0 - \mathbf{p}_k\| \\ & \quad + \|\mathbf{p}^0 - \mathbf{p}_1\| - \mu \cdot c \cdot \bar{S}_k)^2 \\ & = \arg \min_{\mathbf{p}} \frac{1}{\mu^2} \sum_{k=2}^K (\|\mathbf{p} - \mathbf{p}_k\| - \|\mathbf{p} - \mathbf{p}_1\| - \|\mathbf{p}^0 - \mathbf{p}_k\| \\ & \quad + \|\mathbf{p}^0 - \mathbf{p}_1\| - \mu \cdot c \cdot \bar{S}_k)^2 \\ & \arg \min_{\mathbf{p}} \sum_{k=2}^K \left( \frac{1}{\mu} \|\mathbf{p} - \mathbf{p}_k\| - \frac{1}{\mu} \|\mathbf{p} - \mathbf{p}_1\| - \frac{1}{\mu} \|\mathbf{p}^0 - \mathbf{p}_k\| \right. \\ & \quad \left. + \frac{1}{\mu} \|\mathbf{p}^0 - \mathbf{p}_1\| - c \cdot \bar{S}_k \right)^2. \end{aligned} \quad (\text{A.1})$$

For a generic position vector  $\mathbf{p} = [x, y]$  in the standard reference system denote by  $\mathbf{q} \stackrel{\text{def}}{=} \frac{1}{\mu} \cdot \mathbf{p} = [\frac{x}{\mu}, \frac{y}{\mu}]$  the corresponding vector in a new reference system rescaled by  $\frac{1}{\mu}$ . Note that the distance between two point vectors in the new system is also rescaled by the same factor, i.e.,  $\|\mathbf{q}_1 - \mathbf{q}_2\| = \sqrt{(\frac{x_1 - x_2}{\mu})^2 + (\frac{y_1 - y_2}{\mu})^2} = \frac{1}{\mu} \|\mathbf{p}_1 - \mathbf{p}_2\|$ , therefore the problem (A.1) is equivalent to:

$$\begin{aligned} & \arg \min_{\mathbf{q}} \sum_{k=2}^K (\|\mathbf{q} - \mathbf{q}_k\| - \|\mathbf{q} - \mathbf{q}_1\| - \|\mathbf{q}^0 - \mathbf{q}_k\| \\ & \quad + \|\mathbf{q}^0 - \mathbf{q}_1\| - c \cdot \bar{S}_k)^2, \end{aligned} \quad (\text{A.2})$$

where all vector points are expressed in the new rescaled system. The solution  $\mathbf{q}^*$  of (A.2) corresponds to the solution  $\mathbf{p}^*$  of (A.1) expressed in the new reference system. Since the actual value of  $\mu$  is unknown, we cannot exactly map the point  $\mathbf{q}^*$  back to the original reference system, i.e., we cannot derive  $\mathbf{p}^*$  exactly. However, the relative error  $e_{\mu, \mathbf{p}}$  caused by “interpreting” the coordinates of any generic point  $\mathbf{q}$  in the original reference system is equal to  $|\beta_1|$ :

$$e_{\mu, \mathbf{p}} \stackrel{\text{def}}{=} \frac{\|\mathbf{q} - \mathbf{p}\|}{\|\mathbf{p}\|} = \frac{\|\frac{1}{\mu} \cdot \mathbf{p} - \mathbf{p}\|}{\|\mathbf{p}\|} = \left| \frac{1}{\mu} - 1 \right| = |\beta_1|. \quad (\text{A.3})$$

From this proof we can conclude that the DTDoA system is practically *insensitive to a small common frequency offset* (with respect to the nominal frequency) affecting all nodes. On the other hand, DTDoA is extremely sensitive to even small *relative frequency offsets* between the nodes. For this reason, it is important to estimate and compensate for the *relative differences* in clock skew terms, that in our method is achieved by preliminary estimation of and rescaling by  $\hat{\gamma}_k$  (ref. Section 2.4). The penalty for skipping this phase—equivalently, neglecting the presence of independent clock skew terms in the clock error model—is a dramatic increase in the final position error: to illustrate, we report in Fig. A.10 the error distribution that is obtained from the GARDEN data, in the same setting of Fig. 8(a), when skipping the skew correction phase. Comparing Fig. 8(a) and Fig. A.10 (note the

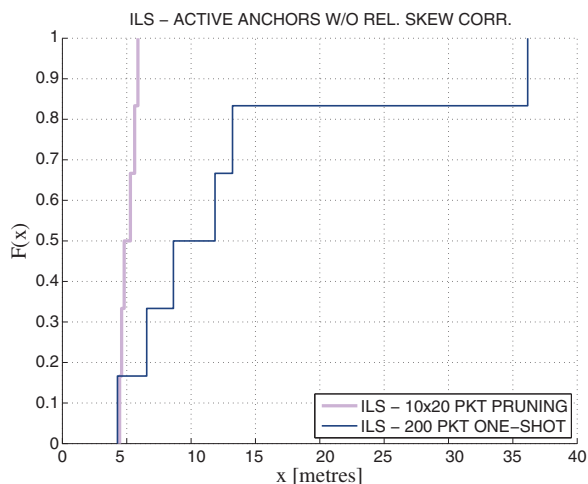


**Fig. A.10.** Distribution of absolute positioning error obtained in the same conditions of Fig. 8(a) but without skew correction.

different horizontal scale) we observe a 10-fold increase of the median S&P error, while the worst-case error with one-shot procedure jumps from 1.4 to 36 m. This confirms the importance of estimating and adjusting for (relative) clock skews.

## References

- [1] Fraunhofer, Awiloc, Available at <http://www.iis.fraunhofer.de/en/bf/ln/technologie/rssi.html>.
- [2] A. Haerlen, E. Flannery, A.M. Ladd, A. Rudys, D.S. Wallach, L.E. Kavraki, Practical robust localization over large-scale 802.11 wireless networks, in: ACM MobySYS, 2004.
- [3] A. Coluccia, F. Ricciato, A software-defined radio tool for experimenting with RSS measurements in IEEE 802.15.4: implementation and applications, in: Fifth IEEE Int'l Workshop on Sensor Networks, 2012.
- [4] D. Han, D.G. Andersen, M. Kaminsky, K. Papagiannaki, S. Seshan, Access point localization using local signal strength gradient, in: ACM PAM, 2009.
- [5] S. Coleri Ergen, H.S. Tetikol, M. Kontik, R. Sevlian, R. Rajagopal, P. Varaiya, RSSI-fingerprinting-based mobile phone localization with route constraints, IEEE Trans. Vehicular Technol. 63 (1) (2014).
- [6] Y. Kim, H. Shin, Y. Chon, H. Cha, Smartphone-based Wi-Fi tracking system exploiting the RSS peak to overcome the RSS variance problem, Pervasive Mobile Comput. 9 (3) (2013).
- [7] S.H. Fang, C.H. Wang, A dynamic hybrid projection approach for improved Wi-Fi location fingerprinting, IEEE Trans. Vehicular Technol. 60 (3) (2011).
- [8] D. Dardari, A. Conti, U. Ferner, A. Giorgetti, M.Z. Win, Ranging with ultrawide bandwidth signals in multipath environments, Proc. IEEE 97 (2) (2009).
- [9] F. Sivrikaya, Y. Bulent, Time synchronization in sensor networks: a survey, IEEE Netw. 18 (4) (2004).
- [10] B. Alavi, K. Pahlavan, Modeling of the TOA-based distance measurement error using UWB indoor radio measurements, IEEE Commun. Lett. 10 (4) (2006).
- [11] N.A. Alsindi, B. Alavi, Measurement and modeling of ultrawideband TOA-based ranging in indoor multipath environments, IEEE Trans. Vehicular Technol. 58 (3) (2009).
- [12] D. Giustiniano, S. Mangold, Caesar: carrier sense-based ranging in off-the-shelf 802.11 wireless LAN, in: ACM CoNEXT, 2011.
- [13] K. Yang, J. An, X. Bu, G. Sun, Constrained total least-squares location algorithm using time-difference-of-arrival measurements, IEEE Trans. Vehicular Technol. 59 (3) (2010).
- [14] S.C.K. Herath, P.N. Pathirana, Robust localization with minimum number of TDoA measurements, IEEE Signal Process. Lett. 20 (10) (2013).
- [15] R. Krishna, C. Hoene, Calculating relative clock drifts using IEEE 802.11 beacons, in: IEEE INDICON, 2009.
- [16] P. Gallo, D. Garlisi, F. Giuliano, F. Gringoli, I. Tinnirello, WMPS: a positioning system for localizing legacy 802.11 devices, IEEE Trans. Smart Process. Comput. (2013).
- [17] C. Hoene, J. Willmann, Four-way TOA and software-based trilateration of IEEE 802.11 devices, in: Personal, Indoor and Mobile Radio Communications, 2008.
- [18] Y. Wang, X. Ma, G. Leus, Robust time-based localization in asynchronous networks, IEEE Trans. Signal Process. 59 (9) (2011).
- [19] R.M. Vaghefi, R.M. Buehrer, Asynchronous time-of-arrival-based source localization, in: IEEE ICASSP, 2013.
- [20] R. Kim, T. Ha, D. Jung, TDoA localization for wireless networks with imperfect clock synchronization, in: IEEE ICIN, 2014.
- [21] B. Liu, H. Chen, Z. Zhong, V. Poor, Asymmetrical round trip based synchronization-free localization in large-scale underwater sensor networks, IEEE Trans. Wireless Commun. 9 (11) (2010).
- [22] D. Zachariah, A. De Angelis, S. Dwivedi, P. Haendel, Schedule-based sequential localisation in asynchronous wireless networks, EURASIP J. Adv. Signal Process. (2014).
- [23] M.R. Gholami, S. Gezici, E.G. Strom, Range-based sensor node localization in the presence of unknown clock skews, in: IEEE ICASSP, 2013.
- [24] T. Li, A. Ekpenyong, Y.-F. Huang, Source localization and tracking using distributed asynchronous sensors, IEEE Trans. Signal Process. 54 (10) (2006).
- [25] S. Dattoo, How tracking customers in-store will soon be the norm. <http://www.theguardian.com/technology/datablog/2014/jan/10/how-tracking-customers-in-store-will-soon-be-the-norm>, 2014.
- [26] F. Ricciato, Time to timestamp: opportunistic cooperative GNSS augmentation from terrestrial radio timing measurements (2014) submitted for publication.
- [27] C. Tiberius, H. Van Der Marel, J.-M. Sleewaegen, F. Boon, Galileo down to a millimetre: analysing the GIOVE-A/B double difference, Inside GNSS (2008).
- [28] M. Maroti, B. Kusy, G. Balogh, Radio interferometric geolocation, in: ACM SenSys, 2005.
- [29] H. Fan, C. Yan, Asynchronous differential TDoA for sensor self-localization, in: IEEE ICASSP, 2007.
- [30] H. Fan, C. Yan, Asynchronous differential TDoA for non-GPS navigation using signals of opportunity, in: IEEE ICASSP, 2008.
- [31] A. Nagy, R. Exel, P. Loschmidt, G. Gaderer, Time-based localisation in unsynchronized wireless LAN for industrial automation systems, in: IEEE ETFA, 2011.
- [32] B. Xu, G. Sun, R. Yu, Z. Yang, High-accuracy TDoA-based localization without time synchronization, IEEE Trans. Parallel Distrib. Syst. 24 (8) (2013).
- [33] A. Coluccia, F. Ricciato, G. Ricci, Positioning based on signals of opportunity, IEEE Commun. Lett. 18 (2) (2014).
- [34] F. Bandiera, A. Coluccia, G. Ricci, F. Ricciato, D. Spano, TDoA localization in asynchronous WSN, in: IEEE EUC, 2014.
- [35] Y.T. Chan, K.C. Ho, A simple and efficient estimator for hyperbolic location, IEEE Trans. Signal Process. 42 (8) (1994).
- [36] J.B.-Y. Tsui, Fundamentals of Global Positioning System Receivers: A Software Approach, John Wiley & Sons, 2004.
- [37] F. Gringoli, L. Nava, OpenFWWF: open firmware for WIFI networks. Available at <http://www.ing.unibs.it/openfwwf/>.
- [38] D. Berger, F. Gringoli, N. Facchi, I. Martinovic, J. Schmitt, Gaining insight on friendly jamming in a real-world IEEE 802.11 network, in: Proceedings of the Seventh ACM Conference on Security and Privacy in Wireless and Mobile Networks, ACM, 2014.
- [39] P. Salvador, V. Mancuso, P. Serrano, F. Gringoli, A. Banchs, VolPiggy: analysis and implementation of a mechanism to boost capacity in IEEE 802.11 WLANs carrying VoIP traffic, IEEE Trans. Mobile Comput. in press (2014a).
- [40] P. Salvador, L. Cominardi, F. Gringoli, P. Serrano, A first implementation and evaluation of the IEEE 802.11aa group addressed transmission service, ACM SigComm Comput. Commun. Rev. 44 (1) (2014b) 36–41.
- [41] iBeacon, <http://en.wikipedia.com/ibeacon>.
- [42] R.M. Vaghefi, J. Schloemann, R.M. Buehrer, NLOS mitigation in TOA-based localization using semidefinite programming, in: IEEE WPNC, 2013.
- [43] I. Guvenc, C.C. Chong, A survey on TOA based wireless localization and NLOS mitigation techniques, IEEE Commun. Surv. Tutorials 11 (3) (2009).
- [44] S. Hara, D. Anzai, T. Yabu, K. Lee, T. Derham, R. Zemek, Analysis on TOA and TDoA location estimation performances in a cellular system, in: IEEE Int'l Conference on Communications (IEEE ICC 2011), 2011.
- [45] S. Sen, K. Kim, P. Congdon, Avoiding multipath to revive inbuilding WIFI localization, in: MobiSys, 2013.

- [46] F. Winkler, E. Fischer, E. Grass, P. Langendoerfer, An indoor localization system based on DTDoA for different wireless LAN systems, in: *Third Workshop on Positioning, Navigation and Communication*, 2006.
- [47] M. Leng, W. Peng Tay, C.M. Samson See, S. Gulam Razul, M.Z. Win, Modified CRLB for cooperative geolocation of two devices using signals of opportunity, *IEEE Trans. Wireless Commun.* 13 (7) (2014).
- [48] R. Garello, J. Samson, M. Spirito, H. Wymeersch, Peer-to-peer cooperative positioning. part II, hybrid devices with GNSS & terrestrial ranging capabilities, *Inside GNSS* (2012).
- [49] A. Amini, R.M. Vaghefi, J.M. De La Garza, R.M. Buehrer, Improving GPS-based vehicle positioning for intelligent transportation systems, in: *IEEE Intelligent Vehicles Symposium*, 2014.